ELSEVIER

International Journal of Solids and Structures 41 (2004) 1313–1329

INTERNATIONAL JOURNAL OF SOLIDS and STRUCTURES

www.elsevier.com/locate/ijsolstr

Simulation of glass cutting with an impinging hot air jet

A.R. Shahani *, M. Seyyedian

Faculty of Mechanical Engineering, K.N.T. University of Technology, Vafadar-e-Sharghi St., 4th Sq., Tehranpars, P.O. Box 016765-3381, Tehran, Iran

Received 17 June 2003; received in revised form 13 September 2003

Abstract

Thermal cutting of glass sheet due to an impinging hot air jet is simulated and analyzed. Induced thermal stresses due to the moving heat source can be used to stably initiate and attract a crack toward the jet axis. Relative motion between the jet and glass sheet then can be used to cut the glass sheet. This paper presents a theoretical study of this process for straight cuts. Process simulation is accomplished by analyzing the coupled temperature and stress fields together with the fracture mechanics criteria for the crack growth.

A finite element remeshing technique is employed for the analysis and singular elements are used around the crack tip for a more precise computing of the stress intensity factor. It is shown that a certain minimum air jet temperature for a given nozzle velocity and a certain maximum air jet velocity for a given temperature are required for continuous cutting. The results of the simulation show a good agreement with the published results in the literature. However a variating nature is detected for the distance between the crack tip and the air jet nozzle from a starting value to the steady-state one.

1. Introduction

Glass sheet cutting is a very important process in the industrial applications of glass sheets. The usual process is scribing the surface in the first step and then breaking off the edges in the second step. In this process, cutting is usually followed by a grinding operation, removing damaged material.

Several alternative thermal cutting techniques possessing some significant advantages have been developed. Most of these techniques, containing laser cutting, electron beam cutting, plasma jet cutting, etc., operate based on the passing of a moving heat source across the sheet. These techniques may be used in the cutting of metallic and non-metallic materials as well as the glass. Metal cutting (or even cutting of non-metallic materials) with any of the above-mentioned techniques has been widely studied in the literature, either analytically or numerically by Bunting and Cornfield (1975), Modest and Abakians (1986a), Modest and Abakians (1986b), Schulz et al. (1993), Sheng and Joshi (1995), Cai and Sheng (1996), Kuang and Atluri (1985), Kim et al. (1993) and Yu (1997). The base of these studies is the solution of the heat transfer

* Corresponding author. Tel.: +98-217343300; fax: +98-217334338.
E-mail address: shahani@kntu.ac.ir (A.R. Shahani).

0020-7683/$ - see front matter © 2003 Elsevier Ltd. All rights reserved.
doi:10.1016/j.ijsolstr.2003.09.059

equation considering the effect of movement of the heat source in this partial differential equation. The reason for this matter lies in the fact that the cutting process occurs based upon the phase change of the material in the cutting area, i.e., it occurs as a result of melting and/or vaporizing the material.

Thermal cutting of glass has been more or less developed and will get successive applications in future (Buerhop and Weissmann, 1996). Glass cutting with an impinging hot air jet is one of these techniques, which operates by establishing a thermal stress field in the glass allowing stable propagation of a pre-existing crack. The advantages of this technique are that intricate and curved shapes and also thick sections can be cut and superior edge quality is obtained. In spite of the advantages of the glass cutting with impinging hot air jet, the only systematic research on simulating the process found in the literature is that of the Muralidhar et al. (1999). This paper presented a theoretical and experimental study of the process for straight cuts. The related quasi-static thermoelasticity problem was analyzed by FEM and temperature and stress fields in the sheet were obtained. The main disadvantage of this work is that the stress analysis is performed without the presence of the crack and thus it is unable to predict the variations of the stand-off distance, which is the distance between the crack tip and heat source after the crack starts to propagate, during cutting process. Also, it cannot predict if the crack growth (i.e., cutting) continues or stops, after being started at first.

In this paper, the attempt is made toward gaining a mathematical model compatible with the actual process. In this regard, the governing equations of the problem, i.e., the quasi-static coupled thermoelasticity equations are derived in accordance with the moving nature of the non-concentrated heat source. The finite element modelling is then accomplished with the standard FE code ANSYS 5.4. The quarter point singular elements are used around the crack tip. Since the crack is to propagate, a remeshing technique is used in each crack extension step. For this to be achieved, ANSYS Parametric Design Language, APDL, is employed. Finally the temperature and stress distributions in the sheet and the variations of the stress intensity factor at the crack tip due to the movement of the heat source are obtained and the effects of the velocity and temperature of the hot air jet on starting and continuance of the cutting process are studied. It is shown that the stand-off distance increases until it reaches a steady-state value, in the cases where cutting is possible.

2. Physical model of thermal cutting of glass

Fig. 1 shows the physical model of the glass thermal cutting process. A sheet of thickness H is to be cut via a moving hot air jet. A pre-crack exists in the plane of symmetry of the glass sheet. Hot air-jet impinges on the glass sheet through a nozzle as shown in the figure. The heat source moves with a constant velocity u on a straight path within the plane of symmetry of the sheet.

A fixed coordinate system xyz is selected at the plane of symmetry, the origin of which lies on the crack mouth on the edge of the sheet, and a moving coordinate system XYZ, moving with the hot air jet nozzle, lies at the same plane with an origin on the lower surface of the sheet.

Due to continuous motion of the heat source with a proper constant velocity and a sufficient air temperature, the pre-crack starts to propagate after the heat source exceeds a certain distance in front of the crack tip. During cutting, the crack tip trails the heat source at a stand-off distance. It will be shown that this distance is not constant and varies with time until it reaches a steady-state value.

3. Mathematical formulation of the problem

The glass cutting process should be accomplished in a certain range of relatively low velocities, in order to have a continuous cutting. This implies that the process should be considered as a quasi-static one. Therefore the governing equations of the problem are:

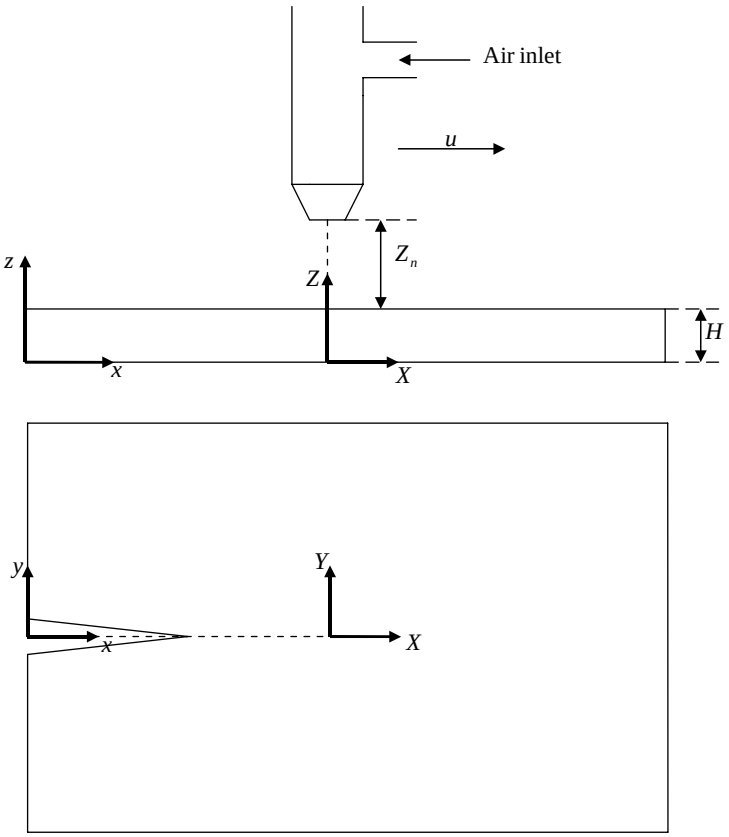

Fig. 1. Schematic model of the thermal cutting.

$$\sigma_{ij,j} = 0 \quad i,j = 1,2,3$$
$$kT_{,ii} = \rho C_p \frac{\partial T}{\partial t} \tag{1}$$

where k is the thermal conductivity coefficient, C_p the specific heat and ρ the density of the glass. Eqs. (1) are the well-known quasi-static equations of thermoelasticity. The associated boundary and initial conditions can be classified as follows.

4. Thermal boundary and initial conditions

The temperature distribution is generally a function of coordinates and time, $T(x,y,z,t)$. It is assumed that the glass sheet is initially at the ambient temperature, T_∞:

$$T(x,y,z,0) = T_\infty \tag{2}$$

Heat transfer occurs between the glass sheet and the air at the top and bottom surfaces. The heat convection through the thin edges of the sheet may be neglected. When there is a single hot air-jet impinging on the top surface, heat transfer from the bottom surface can be neglected, because of the vast difference in heat transfer coefficients of the two surfaces. However, the analysis can easily be extended to the case where

there are jets on both surfaces. For the present case, the boundary conditions on the top and bottom surfaces are:

$$\begin{aligned} k\frac{\partial T}{\partial z}\bigg|_{z=H} &= h(T_a - T_s) \\ k\frac{\partial T}{\partial z}\bigg|_{z=0} &= 0 \end{aligned} \tag{3}$$

where $h = h(x,y)$ is the distribution of the heat convection coefficient on the top surface, T_a the air temperature distribution on the top surface, and $T_s = T(x,y,H,t)$ is top surface temperature distribution. It is obvious that at locations far from the heat source, $T_a \to T_\infty$.

5. Mechanical boundary conditions

Traction-free boundary conditions are assumed on the top and bottom surfaces and on all edges of the sheet including the crack surfaces.

6. Thickness-averaged formulation of the problem

Following the same approach of Muralidhar et al. (1999) the problem can be formulated on a thickness-averaged base. Since the thickness of the glass sheet is small compared with the other dimensions and no traction acts perpendicular to the sheet, the stress analysis reduces to a plane stress analysis of the glass sheet.

On the other hand, the thermal conduction analysis corresponding to the second of Eq. (1) may also be reduced to a two-dimensional one using the thickness-averaging technique. Integrating this equation across the thickness of the sheet and dividing the resultant equation by the thickness H, we have

$$\frac{1}{H}\int_0^H k\nabla^2 T\,\mathrm{d}z = \frac{1}{H}\int_0^H \rho C_p \frac{\partial T}{\partial t}\,\mathrm{d}z \tag{4}$$

Defining the thickness-averaged temperature as

$$\overline{T}(x,y,t) = \frac{1}{H}\int_0^H T(x,y,z,t)\,\mathrm{d}z \tag{5}$$

and assuming constant thermal conductivity, k, we obtain after using Eqs. (3)

$$\frac{1}{H}\int_0^H \frac{\partial^2 T(x,y,z,t)}{\partial z^2}\,\mathrm{d}z = \frac{1}{H}\left(\frac{\partial T}{\partial z}\bigg|_{z=H} - \frac{\partial T}{\partial z}\bigg|_{z=0}\right) = \frac{h}{kH}(T_a - T_s) \tag{6}$$

Substituting this result into Eq. (4), yields

$$k\nabla^2\overline{T} + \frac{h}{H}(T_a - T_s) = \rho C_p \frac{\partial \overline{T}}{\partial t} \tag{7}$$

In this equation the Laplacian operator stands for $\nabla^2 = \frac{\partial^2}{\partial x^2} + \frac{\partial^2}{\partial y^2}$. With the applied averaging technique we can say:

$$T_s = \overline{T}(x,y,t) \tag{8}$$

This assumption is valid for thin plates, but can be improved considerably by assuming that the temperature variations along the z-direction are approximated by a function $f(z)$ as

$$f(z) = Az^2 + Bz + C \tag{9}$$

With this definition, the top surface temperature may be computed

$$T_s = T(x, y, H, t) = AH^2 + BH + C \tag{10}$$

Substituting Eq. (9) into Eq. (5) results in

$$\bar{f} = \overline{T}(x, y, t) = \left(\frac{A}{3}\right)H^2 + \left(\frac{B}{2}\right)H + C \tag{11}$$

Assuming the boundary conditions on the top and bottom surfaces of the plate, Eq. (3), in conjunction with the assumed distribution of temperature in Eq. (9), we obtain

$$\left.\frac{\partial f}{\partial z}\right|_{z=0} = B = 0 \tag{12}$$

$$\left.\frac{\partial f}{\partial z}\right|_{z=H} = 2AH + B = \frac{h}{k}(T_a - T_s) \tag{13}$$

From Eqs. (11)–(13) the constants A, B and C may be obtained in terms of the boundary conditions, which can be substituted into Eqs. (9) and (10) to give

$$T_s = \frac{NuT_a + 3\overline{T}(x, y, t)}{3 + Nu} \tag{14}$$

where

$$Nu = \frac{hH}{k} \tag{15}$$

is the local Nusselt number. When $Nu \ll 1$, the sheet can not support temperature gradients through the thickness and Eq. (14) reduces to Eq. (8). When heat transfer is dominated by convection ($Nu \gg 3$),

$$T_s = T_a(x, y, t) \tag{16}$$

Substituting Eq. (14) into Eq. (7) results in

$$k\nabla^2\overline{T}(x, y, t) + \frac{3}{3 + Nu}\left(\frac{h}{H}\right)(T_a - \overline{T}(x, y, t)) = \rho C_p \frac{\partial \overline{T}}{\partial t} \tag{17}$$

The advantage of Eq. (17) is that it is expressed in terms of the average temperature $\overline{T}$ and the air temperature T_a.

7. Distribution of heat-convection coefficient and air temperature

The distribution of the heat transfer coefficient and air temperature is dependent on many process parameters including nozzle diameter (D), the distance between the nozzle exit and the glass sheet (Z_n) and air jet velocity (u). Muralidhar et al. (1999) give the following relation for the heat convection coefficient according to the previous extensive investigations (Gardon and Cobonpue, 1962 and Hrycak, 1983):

$$\frac{h(r)-h_\infty}{h_o-h_\infty}=\exp\left[-\left(\frac{r}{b_h}\right)^n\right] \tag{18}$$

where r is the radial distance from the nozzle axis, h_o the stagnation point heat convection coefficient (at $r=0$), h_∞ its value far from the heat source, b_h a characteristic decay distance, and n a characteristic exponent. The maximum value of h_o is achieved for $2<\frac{Z_n}{D}<8$, where D is the nozzle diameter.

Here we have used the values reported for b_h and n by Muralidhar et al. (1999), i.e., $b_h=3.75D$ for $\frac{Z_n}{D}<8$, and also $n=1$. The value of h_o could also be computed from the following relation

$$\frac{h_o D}{k_a}=13Re_o^{0.5}\left(\frac{D}{Z_n}\right) \tag{19}$$

where k_a is the thermal conductivity of air and Re_o is the Reynolds Number based on the exit velocity, v_j, and nozzle diameter, D:

$$Re_o=\frac{v_j D}{\nu^*} \tag{20}$$

where ν^* is the kinematic viscosity of the air. Since the nozzle operates under chocked condition, the exit velocity, which is the sonic velocity, may be computed using the relation:

$$v_j=(\gamma^* R T_e)^{0.5} \tag{21}$$

where $\gamma^*=1.4$ and $R=287$ J/kg °C for the air jet and T_e is the absolute air jet exit temperature.

A similar radial distribution may be used for the air temperature:

$$\frac{T_a(r)-T_\infty}{T_o-T_\infty}=\exp\left[-\left(\frac{r}{b_a}\right)^n\right] \tag{22}$$

where T_o is the stagnation-point temperature, b_a a characteristic decay distance and T_a the air temperature far from the jet. According to Muralidhar et al. (1999) we have $b_a=b_h=b$ and $n=1$.

8. Crack growth criterion

Since glass is a brittle material, the necessary condition for cutting is the brittle fracture criterion, i.e.:

$$K_I \geqslant K_{IC} \tag{23}$$

where K_{IC} is the fracture toughness of the glass. From Eq. (23), the crack length a can be found at any instant of time. On the other hand, it is well-known that at the crack growth stage, the stress component contributing the opening of the crack reaches a critical value, i.e., the ultimate strength of the material.

9. Finite element modeling of the problem

Because of symmetry, only one half of the sheet is modeled by FEM, regarded that the displacement component in the y-direction of the connecting surfaces in the symmetry plane must be confined, Fig. 2. The FE standard code ANSYS 5.4 is used for modeling the problem. Quadratic isoparametric triangular elements are employed for the discretization of the model. In the first step using this type of elements with the single degree of freedom (per node) for temperature (Plane35, ANSYS 5.4, 1997), the thermal analysis of the problem is accomplished. In the second step, the obtained nodal temperatures are introduced as the body forces for the structural analysis. Afterby, the structural analysis is done by the quadratic isoparametric tri-

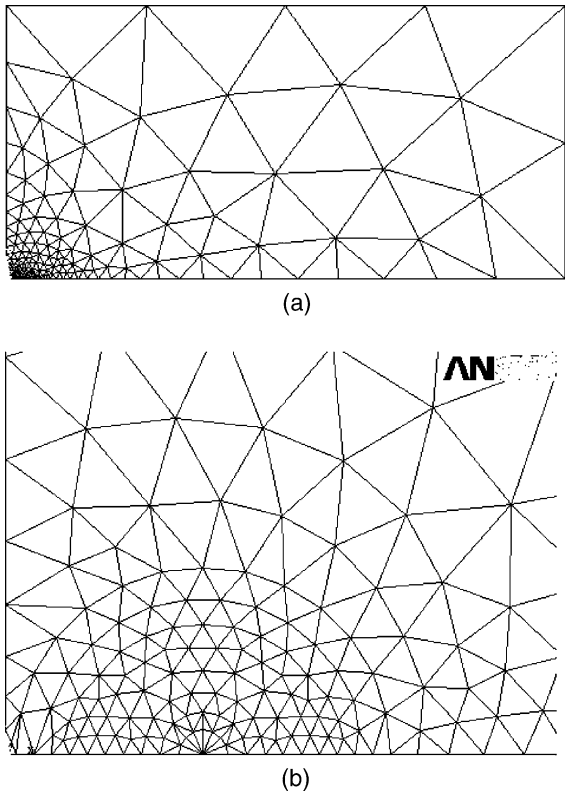

Fig. 2. Finite Element model of the problem. (a) The entire model of half-plane. (b) The meshes generated around the crack tip.

angular elements with two degrees of freedom for each node (Plane2, ANSYS 5.4, 1997). These elements are capable of constructing singular elements, first introduced by Barsoum (1977), which are used for modeling the familiar square root singularity at the crack tip (Fig. 2b). The half plane is discretized by 519 elements.

10. Remeshing technique

Since the loading and geometry of the problem are time-dependent, ANSYS Parametric Design Language, APDL, is used for mesh generation and applying the loads and boundary conditions in each step of time. This time-dependency is due to the movement of the heat source and transient behavior of the temperature distribution in the sheet.

Fig. 3 shows the flow-chart of the prepared APDL program algorithm. The time interval of the analysis is divided into steps of length Δt. Each time step corresponds to an incremental movement of the heat source. After each incremental movement of the heat source, a thermal analysis followed by a structural analysis are accomplished and then the stress intensity factor, K_I, is computed by the software.

Indeed, in each step Δt the heat source is displaced by an amount $u\Delta t$, where, u is the heat source velocity. If the stress component σ_{yy} becomes large enough to cause K_I to exceed K_{IC} in this step, provided that σ_{yy} is a tensile stress, the crack extends and the crack tip moves with an amount $u\Delta t$. Otherwise, the crack does not grow in this step. The accuracy of the method will be assured if the time steps Δt are chosen small enough.

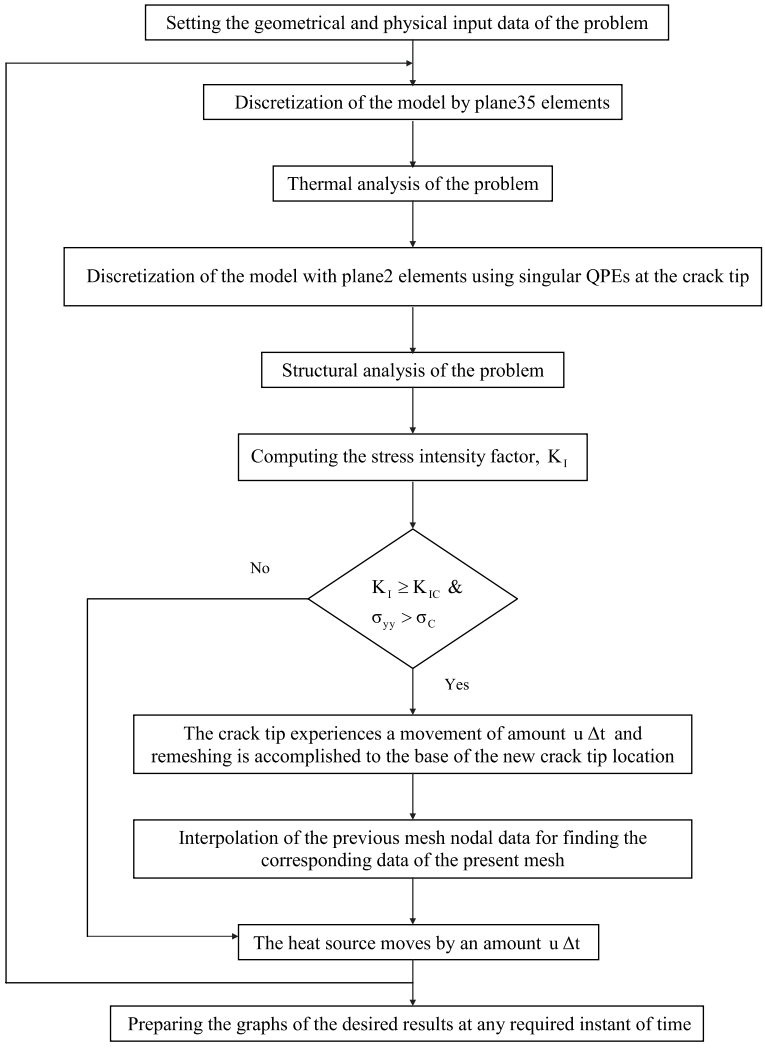

Fig. 3. Flow-diagram of the FEM algorithm of the problem.

If the crack grows in a specific time step, the following finite element analysis of the problem will be proceeded by remeshing of the plate. In fact, remeshing starts from singular elements of the crack tip and thus after each crack growth, a new mesh generation with this start point is done. At this step, the nodal data of the previous mesh should be used to interpolate the corresponding data in the present nodes. These data are then used as the set points of the present FE analysis.

11. Results and discussion

In this part of the paper some numerical examples are considered regarding various parameters affecting the thermal cutting process. Numerical values for the geometry, material properties and processing parameters are given in Table 1. At first, it is assumed that the heat source is fixed over the crack tip ($r = 0$).

Table 1
Numerical values of the problem parameters (Muralidhar et al., 1999)

Parameter	Value
Nozzle diameter, D	1–3 mm
Nozzle height, Z_n	2–10 mm
Maximum air temperature, T_o	37–500 °C
Ambient temperature, T_∞	25 °C
Modulus of elasticity, E	70.6 GPa
Poisson's ratio, υ	0.25
Thermal conductivity, k	0.79 W/m °C
Thermal coefficient expansion, α_t	9.75×10^{-6} /°C
Fracture toughness, K_{IC}	0.5 MPa $\sqrt{m}$
Density, ρ	2500 kg/m^3
Specific heat, C_p	460 J/kg °C
Maximum heat transfer coefficient, h_o	Should be computed from Eq. (19)
Minimum heat transfer coefficient, h_∞	$0.1h_o$
Sheet thickness, H	3–6 mm
Heat source velocity, u	0–6 mm/s
Glass sheet dimensions	1 m×1 m
Softening point temperature of glass	≈600 °C

For a sheet thickness $H = 3$ mm, nozzle diameter $D = 2$ mm, nozzle height $Z_n = 5$ mm and the air stagnation temperature $T_o = 377$ °C, the contours of the temperature around the crack tip at $t = 40$ s are shown in Fig. 4. It is seen that the zone of constant temperature is of circular forms with centers at the crack tip. It is also seen that the observed temperature distribution is local and at a distance not very far from the crack tip the average temperature exceeds the ambient temperature.

Fig. 5 shows the temperature variations along the symmetry line (X-axis) together with the stress distribution along the same line. The parameters were normalized in order to compare the results with the

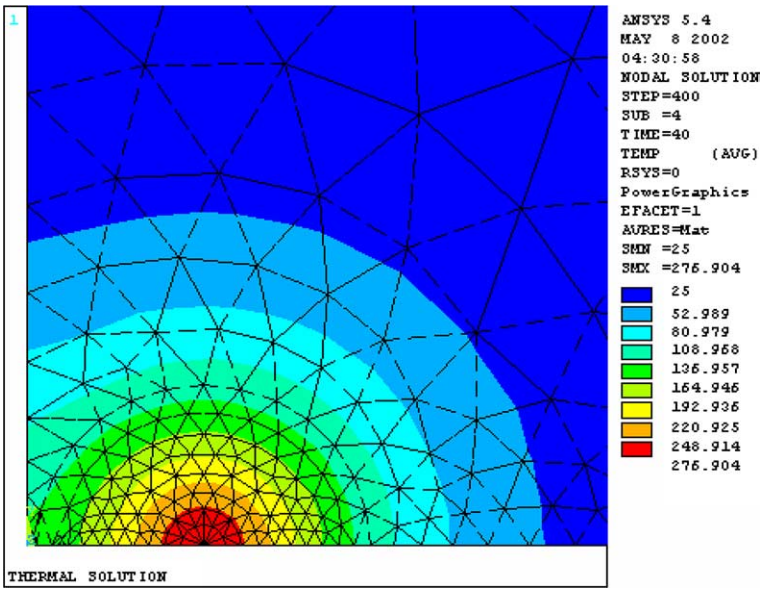

Fig. 4. Temperature contours due to a fixed heat source above the crack tip.

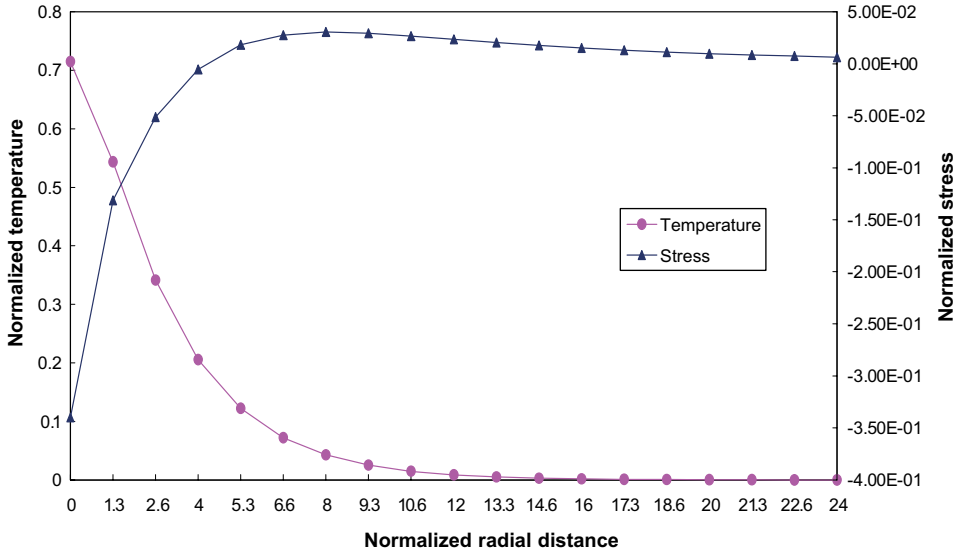

Fig. 5. Normalized temperature and stress distribution versus the distance from the heat source.

Fig. 7 of the simulation of Muralidhar et al. (1999), $\left(X^* = \frac{X}{H},\ T^* = \frac{T-T_\infty}{T_o-T_\infty} \text{ and } \sigma^*_{yy} = \frac{\sigma_{yy}(1-\upsilon)}{E\alpha(T_o-T_\infty)}\right)$. The comparison shows a good qualitative and also quantitative (for the peak and steady-state values) agreement. The difference is because of the unexpected difference in local Nusselt numbers. The results of Fig. 5 are valid for different values of hot air temperature, T_o, in the range 37–377 °C. It is seen from the figure that the stress is compressive at the crack tip and in a certain vicinity of it. Also, the stress has a singular nature at the crack tip. The crack can not extend until the stress at the crack tip is in compressive (closure) mode.

For the purpose of validating the results of the simulation, a comparison is made with the experimental results of Muralidhar et al. (1999). These experimental results include the measured temperatures at the top and bottom surfaces of the glass sheet subjected to a stationary heat source. Fig. 6 shows the results of this comparison. In this figure normalized temperature is plotted as a function of normalized radial distance from the air jet nozzle. The top and bottom surface temperatures from the simulation are plotted using Eqs. (14) and (9), respectively, and the average temperature is also included. It is seen that in the vicinity of the nozzle, the top and bottom surface temperatures show a great difference, but at some distances from the nozzle ($\frac{r}{H} \approx 2$), the top and bottom surface temperatures become the same and equal to the thickness-averaged temperature. Also, it is observed that a relatively good agreement exists between the results of simulation and that of experiment.

Now, we consider a moving heat source starting from the crack tip and traveling along the x-axis. The corresponding temperature distribution is shown in Fig. 7 for a velocity $u = 3$ mm/s and $T_o = 77$ °C, $D = 2$ mm, $Z_n = 4$ mm and $H = 3$ mm at the instant $t = 10$ s. It is apparent from the figure that the contours are stretched in such a manner they become nearer to each other ahead and farther from each other behind the heat source. This result accords with theoretical results of Nowinski (1978).

Fig. 8 gives the temperature distribution along the x-axis for different nozzle velocities under the same condition of Fig. 7 at $t = 40$ s. It is observed that the peak temperature at non-zero nozzle velocities occurs somewhere behind the heat source and this distance from the nozzle axis increases as the velocity increases. Meanwhile, the peak value of temperature decreases as the velocity increases, since a less amount of energy is delivered to the sheet at higher velocities. These results are in agreement with those cited in the literature by Manca et al. (1995) and Manca et al. (1999).

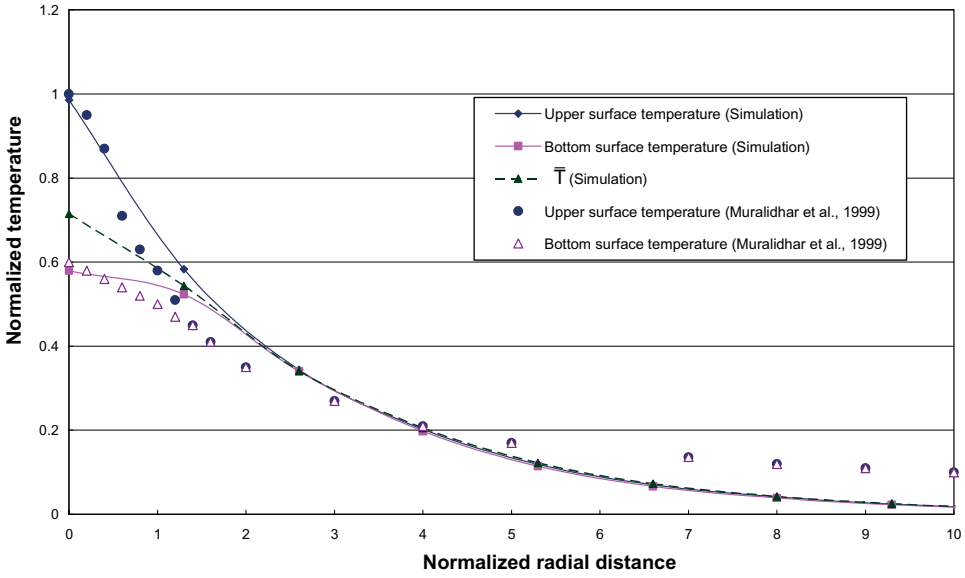

Fig. 6. Comparison of the normalized temperature obtained from simulation with the experimental results of Muralidhar et al. (1999).

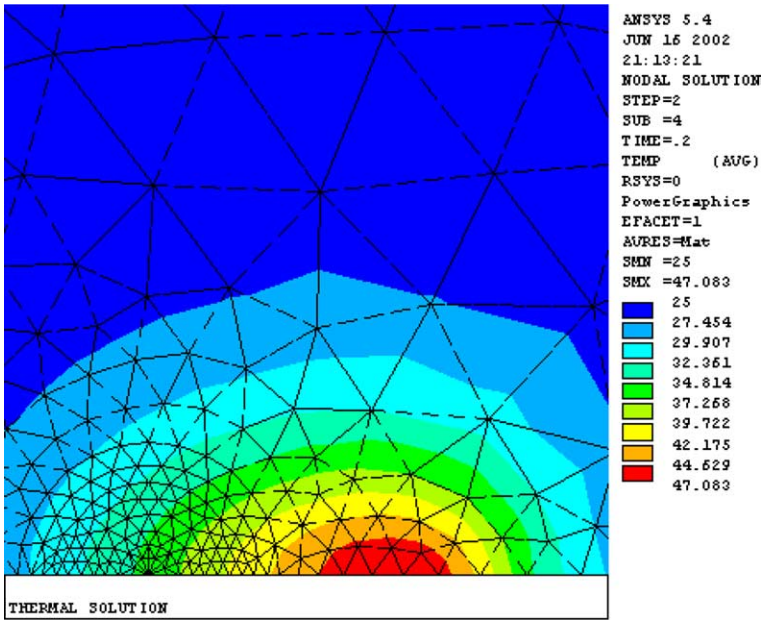

Fig. 7. Temperature contours under a moving hot air jet.

Fig. 9 shows the effect of the velocity of the hot air jet on the stress component, σ_{yy}, at the crack tip, for the air temperature $T_o = 77$ °C. It is seen that for all velocities in the given range 0.3–6 mm/s, σ_{yy} experiences a compressive nature at the crack tip and thus, the crack cannot extend because it is in closure (and not in

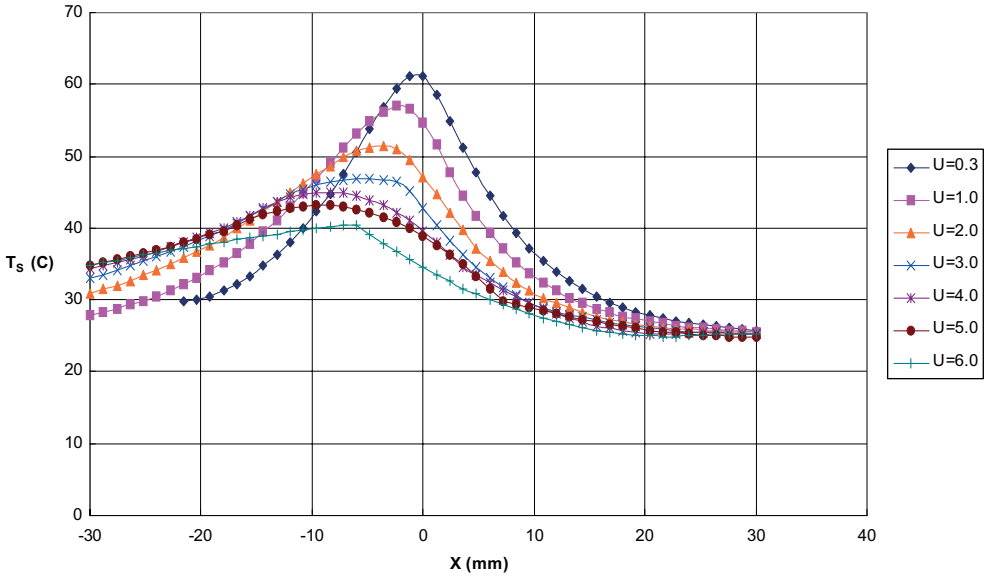

Fig. 8. Temperature distribution for different heat source velocities at $t = 40$ s.

opening) mode. Anyway, after the heat source reaches a certain distance from the crack tip, it changes from compressive to tensile. But the crack propagation does not occur until the stress reaches a critical value, at which the crack starts to propagate. It is observed that this distance is not the same for all values of the heat source velocity and it increases as the velocity increases. These starting values of the "stand-off" distance are given in Table 2.

It is worth mentioning that as the air jet nozzle moves and reaches its certain stand-off distance, the stress component σ_{yy} is a tensile stress with the critical value at the crack tip and always has a compressive nature under the nozzle. In fact, this stress gradient is responsible for the stable crack extension, i.e., stable cutting of the sheet.

It is also seen from Fig. 9 that σ_{yy} remains constant after it takes its critical value. More accurate observation shows that at this air stagnation temperature, $T_o = 77$ °C, the cutting process will be continued only for velocities $u = 0.3$ and 1 mm/s and for other velocities, the stress σ_{yy} at the crack tip ceases to maintain the critical value and this means the cutting stop. It can be concluded that at any given air temperature the start and continuance of the cutting process depend on the heat source velocity.

Fig. 10 gives the stress intensity factor values at the crack tip for different nozzle velocities. It may be seen that as the heat source starts to move from the crack tip, the K_I-value is zero through some distance from the tip at any velocities. This is because, as we saw, the σ_{yy} component at the crack tip has a compressive nature until the nozzle reaches a certain distance from the crack tip. Thus, the crack is in closure mode in this range and the crack opening displacement and hence, the K_I-values are zero. Further, the K_I-value takes a positive value which after experiencing a local maximum, it increases again and reaches a critical value, i.e., the fracture toughness of the glass, K_{IC}. Again, the starting and continual conditions of the cutting process are the same as that discussed about Fig. 9.

The variations of the stand-off distance, a, for different values of nozzle velocities are shown in Fig. 11. The start of the crack extension (i.e., the cutting process) and the according stand-off distance are recognized in the figure, by the first breaking point of the curves, the corresponding values of which were given in the second column of the Table 2. It is also noticeable that, as previously said, the stand-off distance for the

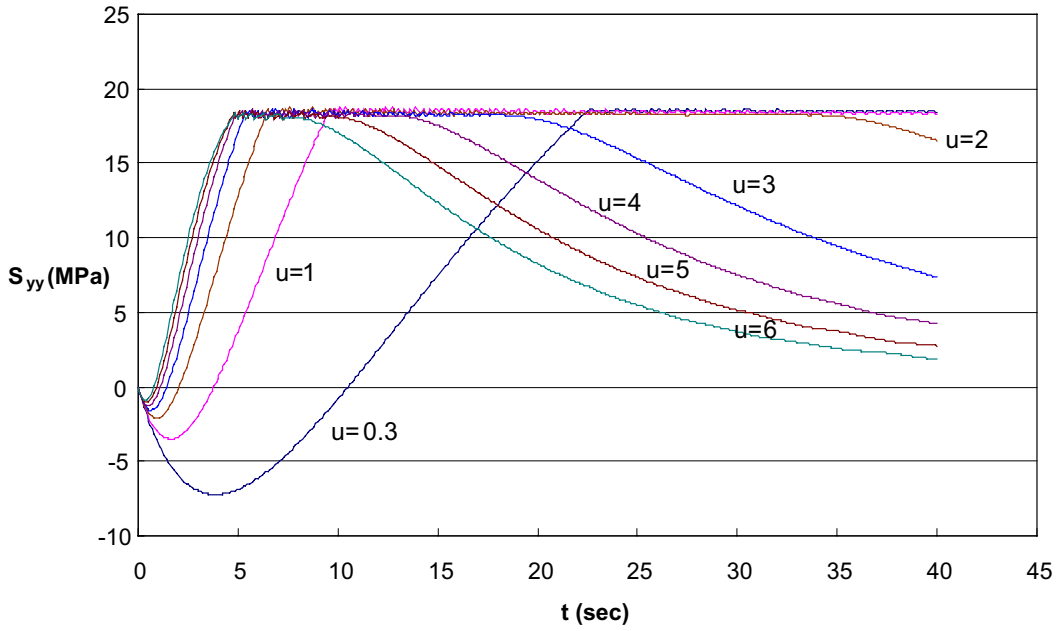

Fig. 9. Variations of the stress component, σ_{yy}-value at the crack tip for different heat source velocities.

Table 2
The starting and steady-state values of the stand-off distance for different heat source velocities for the input data $T_o = 77$ °C, $D = 2$ mm, $Z_n = 4$ mm and $H = 3$ mm

u (mm/s)	Starting value of stand-off distance (mm)	Steady-state value of stand-off distance (mm)
0.3	6.72	7.83
1	9.5	16.7
2	12.8	–
3	15.9	–
4	19.2	–
5	23.5	–
6	28.8	–

nozzle velocities $u = 0.3$ and 1 mm/s increases successively and reaches a steady-state value with which the cutting is continued. This can be described by the transient nature of the temperature distribution in the sheet. Indeed, the temperature field also increases in a transient manner until it takes a steady-state value and hence, the transient nature of the stand-off distance is a consequence of that of the temperature field. The related values of the steady-state stand-off distance are given in the third column of the Table 2. It is seen from the figure that the other curves corresponding to the greater velocities experience another breaking which are related to the cutting process stop. After this point the stand-off distance successively increases, meaning that the crack ceases to extend. The cutting stop is because of successive increase of the stand-off distance resulting in the insufficiency of the stress component σ_{yy} for further crack growth (as may be seen from Fig. 9).

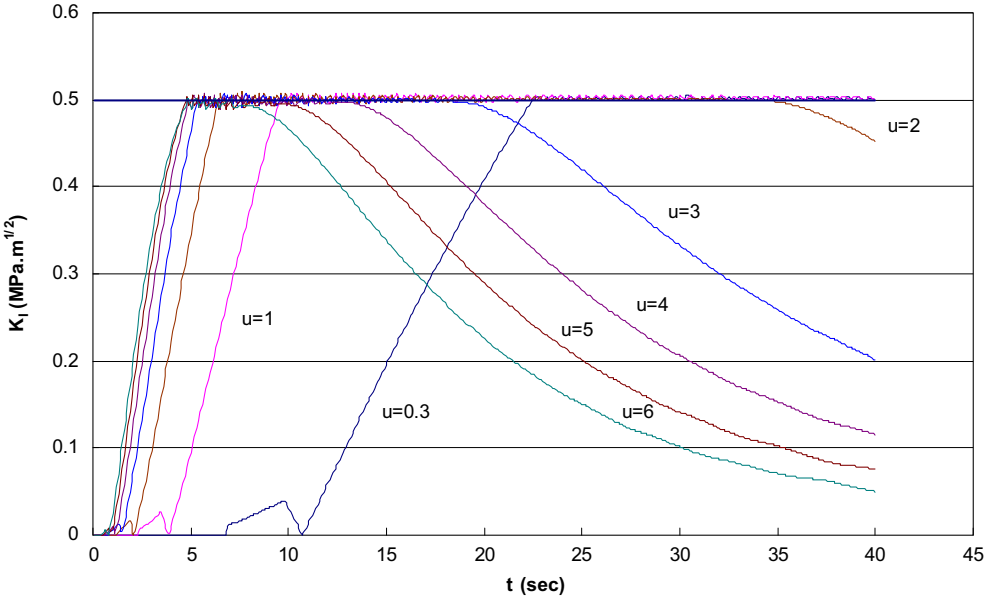

Fig. 10. Variations of the stress intensity factor for different heat source velocities.

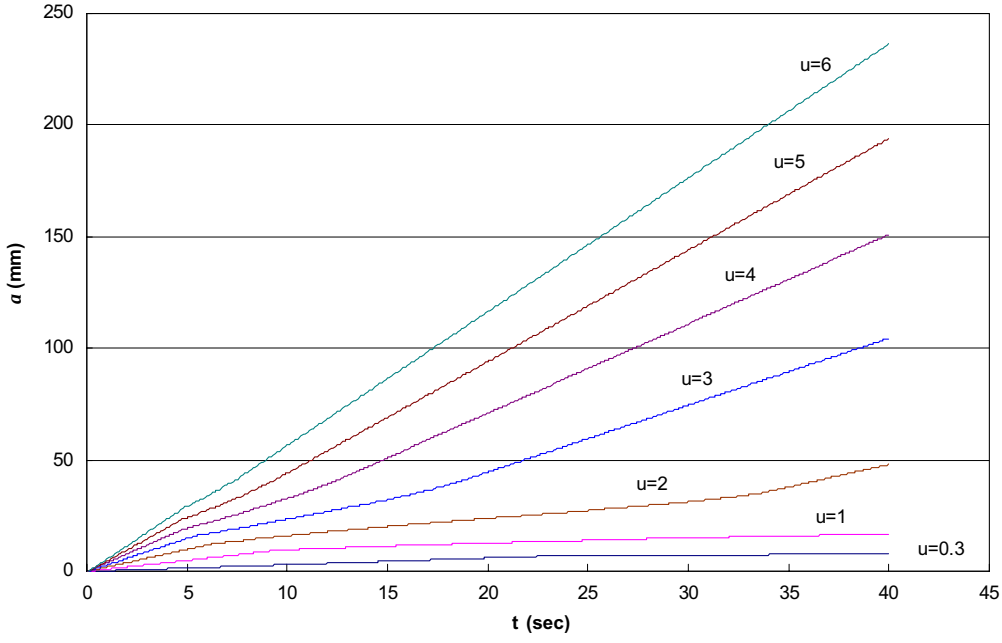

Fig. 11. Variations of the stand-off distance for different velocities.

The effect of air temperature change on the cutting should be studied with the aid of Figs. 12 and 13. The hot air nozzle is considered to travel with a speed $u = 1$ mm/s and the nozzle exit diameter is $D = 2$ mm with

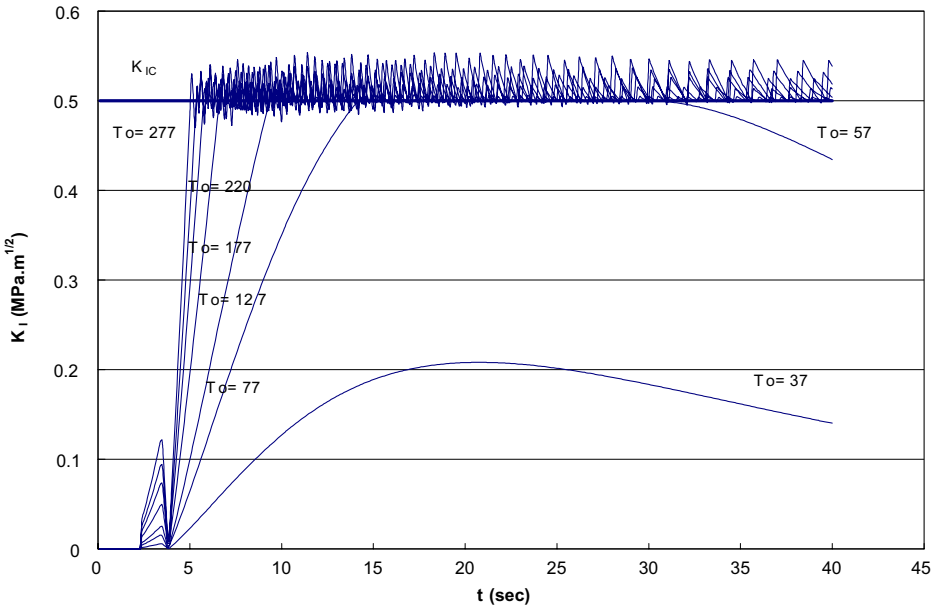

Fig. 12. Effect of air temperature on the variations of the stress intensity factor.

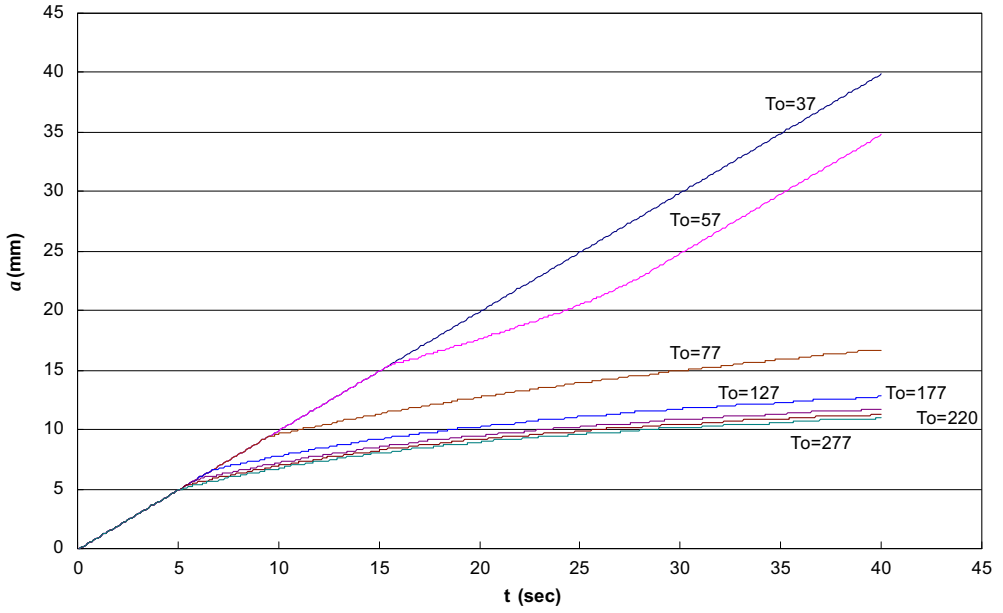

Fig. 13. Variations of the stand-off distance for various air temperatures.

a $Z_n = 2$ mm distance from a $H = 3$ mm thickness sheet. Fig. 12 shows the variation of the stress intensity factor as a function of the air temperature. It is observed that for $T_o = 37$ °C the K_I-curve fully lies below

the $K_I = K_{IC}$ line, meaning that cutting is not possible with this temperature. At a higher temperature $T_o = 57$ °C the K_I-curve intersects the $K_I = K_{IC}$ line at two points. The first point introduces the start of crack extension (cutting) and the second one the point at which cutting ceases to continue. For higher temperatures the K_I-values reach the fracture toughness of the glass and remain constant showing the continuance of the process. Thus, we can conclude that at any given nozzle velocity a certain minimum air temperature is required for the starting and continuance of the cutting process.

The assessment of the cutting process should be better accomplished with the aid of Fig. 13. It can clearly be seen that at the temperature $T_o = 37$ °C, the cutting is impossible, since the 'a'-curve is a 45° angle straight line, the slope of which is the velocity of the nozzle, i.e., unity. At $T_o = 57$ °C, the crack extension starts when the nozzle reaches a certain distance from the crack tip, but stops after some moment. The $T_o = 77$ °C is a temperature at which continuous cutting is possible. At any higher temperature, continuous cutting occurs. It may be observed that the higher the air temperature, the smaller the starting and the steady-state values of the stand-off distance.

The results of simulation show that the effect of the variations of the nozzle height from the sheet is small in the range $2 < \frac{Z_n}{D} < 8$, (the graphs of which are not given here for the sake of brevity), which are in accordance with the experimental results of Muralidhar et al. (1999).

12. Conclusions

The problem of straight line cutting of glass sheets by an impinging hot air jet has been analyzed by the coupled quasi-static thermoelasticity theory and fracture mechanics. A remeshing technique in the FEM context is used based on the propagating characteristics of the crack. The results of the analysis have been in good agreement with the published results in the literature. The following conclusions have been made from the above-mentioned simulation of the cutting process:

- As the hot air jet nozzle starts to move from the crack tip, the crack tip falls into the induced compression zone via the heat source, to some extent of the travel of the nozzle and thus the crack cannot extend in this range. After the nozzle reaches a certain stand-off distance, the crack may start to propagate (if the cutting requirements are fulfilled), which may be regarded as the start of cutting. Indeed, there exists a stress (σ_{yy}) gradient, from the tensile critical value at the crack tip to the compressive stress under the heat source, causing the stable crack propagation, i.e., the stable cutting.
- The stand-off distance is not a constant value and may vary from its starting value to the steady-state value (if the cutting is possible). These variations could be understood keeping the transient nature of the temperature distribution in mind.
- For the case when the cutting is impossible, two different cases can be distinguished:
  (i) The requirements for the start of cutting (explained later) are not met and so the cutting could not be started at all.
  (ii) The cutting is started because of the fulfillment of its requirements, but could not be continued due to the reduction of the stress intensity factor from its critical value. This reduction may be caused by the successive increase of the stand-off distance, which makes the stress σ_{yy} not to be sufficient for the further crack growth.
- For a given nozzle velocity, a certain minimum air temperature is required for the starting and continuance of the cutting process, in an acceptable range of the nozzle height from the glass sheet.
- At a certain air temperature with a reasonable range of the nozzle height from the sheet, the start and continuance of the cutting process depends on the heat source velocity. In fact, the nozzle velocity is confined to a certain maximum value.
- The effect of the variations of the nozzle height from the sheet is small in the range $2 < \frac{Z_n}{D} < 8$.

- For a given air temperature, the higher the nozzle velocity, the larger the starting and steady-state values of the stand-off distance.
- For a given nozzle velocity, the higher the air temperature, the smaller the starting and steady-state values of the stand-off distance.

Acknowledgement

The authors would like to acknowledge the financial support of the research deputy of the K.N.T. University of Technology.

References

ANSYS 5.4 User's Manual, 1997. Swanson Analysis Systems, Inc., Pennsylvania.

Barsoum, R., 1977. Triangular quarter-point elements as elastic and perfectly-plastic crack tip elements. International Journal for Numerical Methods in Engineering 11, 85–98.

Buerhop, C., Weissmann, R., 1996. Temperature Development of Glass during CO_2 Laser Irradiation. Part 1. Measurement and Calculation. Glass Technology 37 (2), 69–73.

Bunting, K.A., Cornfield, G., 1975. Toward a general theory of cutting: a relationship between the incident power density and the cut speed. Journal of Heat Transfer, Transaction ASME (Feb), 116–122.

Cai, L., Sheng, P., 1996. Analysis of laser evaporative and fusion cutting. Journal of Manufacturing Science and Engineering 118, 225–234.

Gardon, R., Cobonpue, J., 1962. Heat transfer between a flat plate and jets of air impinging on it. In: Proceedings of the Heat Transfer Conference, International Developments in Heat Transfer (Part II, London). ASME, New York, pp. 454–460.

Hrycak, P., 1983. Heat transfer from round impinging jets to a flat plate. International Journal of Heat and Mass Transfer 26 (12), 1857–1865.

Kim, M.J., Chen, Z.H., Majumdar, P., 1993. Finite element modeling of the laser cutting process. Computers and Structures 49 (2), 231–241.

Kuang, Z.-B., Atluri, S.N., 1985. Temperature field due to a moving heat source: a moving mesh finite element analysis. Journal of Applied Mechanics, Transaction ASME 52, 275–280.

Manca, O., Morrone, B., Naso, V., 1995. Quasi-steady-state three-dimensional temperature distribution induced by a moving circular gaussian heat source in a finite depth solid. International Journal of Heat Mass Transfer 38 (7), 1305–1314.

Manca, O., Morrone, B., Nardini, S., 1999. Thermal analysis of solids at high Peclet numbers subjected to moving heat sources. Journal of Heat Transfer, Transaction ASME 121, 182–186.

Modest, M.F., Abakians, H., 1986a. Evaporative cutting of a semi-infinite body with a moving CW laser. Journal of Heat Transfer, Transaction ASME 108, 602–607.

Modest, M.F., Abakians, H., 1986b. Heat conduction in a moving semi-infinite solid subjected to pulsed laser irradiation. Journal of Heat Transfer, Transaction ASME 108, 597–601.

Muralidhar, S., Pal, S., Jagota, A., Kale, S.R., Mittal, R.K., 1999. A study of thermal cutting of glass. Journal of American Ceramic Society 82 (8), 2166–2176.

Nowinski, J.L., 1978. Theory of Thermoelasticity with Applications. Sijthoff & Noordhoff International Publishers, The Netherlands.

Schulz, W., Becker, D., Franke, J., Kemmerling, R., Herziger, G., 1993. Heat conduction losses in laser cutting of metals. Journal of Physics D, Applied Physics 26, 1357–1363.

Sheng, P.S., Joshi, V.S., 1995. Analysis of heat-affected zone formation for laser cutting of stainless steel. Journal of Materials Processing Technology 53, 879–892.

Yu, L.M., 1997. Three-dimensional finite element modeling of laser cutting. Journal of Materials Processing Technology 63, 637–639.